Aperture Sharing Metasurface-Based Wide-Beam Antenna for Energy Harvesting

Wenzhang Zhang [a,b], Jinyao Zhang [b], Chaoyun Song [c], Rui Pei [d], Xuanming Zhang [e], Haiwen Liu [f], Congzheng Han [g], Huang Yi [b], Jiafeng Zhou [b]

[a] *School of Internet of Things, Xi'an Jiaotong-Liverpool University, Suzhou, China*
[b] *Department of Electrical Engineering and Electronics, University of Liverpool, Liverpool, L69 3GJ, U.K.*
[c] *Department of Engineering, King's College London, London, U.K.*
[d] *College of Information Science and Technology, Donghua University, Shanghai, China*
[e] *Xi'an University of Posts & Telecommunications, School of Electronic Engineering, Xi'an, China*
[f] *Xi'an Jiaotong University, Xi'an, China*
[g] *Institute of Atmospheric Physics, Chinese Academy of Sciences, Beijing, China*

A R T I C L E I N F O

Keywords:
Energy harvesting
Metasurface (MTS) antenna
Rectenna
Wide beamwidth

A B S T R A C T

Since the available ambient power level is usually quite low for radio frequency energy harvesting, it is very desirable for an antenna to have both a high gain and a wide beamwidth performance. Usually, they cannot be achieved simultaneously. In order to overcome this limitation, a multi-port antenna using a nonuniform metasurface (MTS) is presented. In this MTS-based antenna, three modes with complementary radiation patterns are excited through one middle and two side aperture-coupled feeding ports. The first mode is the fundamental TM_{10} mode with in-phase current distributions on the MTS. It has a broadside directional radiation pattern with a high gain. The second and third modes are symmetrical to each other at a high mode. They have opposite current distributions on two sides of the MTS. These two modes have a directional radiation pattern with a tilted angle. These three modes share the same aperture but are excited by three different feeds. Each feed is connected to a rectifier. By combining direct current (DC) output to a single load, an antenna with a wide beam and a high gain can be effectively achieved, although each mode has the usual limitation of gain and beamwidth. The key advantage of this proposed rectenna is that the unit cells on the MTS layer can be reused to excite different MTS modes with different radiation patterns simultaneously. Thus, a wide beamwidth can be achieved. Three realized beams are oriented at -35°, 0°, and +35° respectively. By combining the DC output from the three modes, the proposed rectenna has effectively achieved a beamwidth of 114° with a gain ranging from 8 to 9.8 dBi. The RF-to-DC conversion efficiency of the rectifiers is 3%-67% at 2.45 GHz when the input power ranges from -35 to 0 dBm. The proposed MTS antenna with an overall size of $\lambda_0 \times \lambda_0 \times 0.03\ \lambda_0$ can achieve 12% fractional bandwidth.

* Corresponding author.

1. Introduction

With the fast growth of the internet of things (IoT), a massive number of batteries will be required to charge billions of IoT devices. These batteries will be continuously charged and replaced, which is too time- and source-consuming. To deal with this problem, researchers have explored the technique of radio frequency (RF) energy harvesting (EH), which can be complementary to the battery in a reliable system and can even replace batteries in some low-power scenarios. RF EH employs a rectenna, which consists of an antenna, a matching network, and a rectifying circuit with semiconductor devices (e.g., diodes). The overall performance of a rectenna is mainly decided by the properties of the antenna and the efficiency of the rectifying circuit [1]-[2]. In reality, if the antenna does not receive enough power, the rectenna efficiency may be less than ideal. Since ambient electromagnetic signals are normally available at low power levels in different directions. One solution to improve the input power level is adopting wide-beam or multi-beam antennas [3], to effectively exploit incident RF waves from different directions.

However, if a wide-beam antenna with one port is used to collect the power from radio waves, the antenna will be inevitably with a low gain, resulting in low sensitivity owing to the low power density. This is due to the fact that, for a one-port antenna, the gain is normally inversely proportional to the beamwidth [4].

To resolve this problem, the utilization of a wide-beam (or multi-beam) antenna with multiple ports could be a solution. By using multiple ports, the potential of the antenna aperture can be maximized since each port can be assigned to excite one beam focusing on one direction. Several wide-beam (or multi-beam) antennas with multiple ports have been presented for RF energy harvesting systems recently [5]-[6]. In [5], a scheme integrating the coupled patch antenna and the hybrid coupler was introduced. The beamforming circuit was simpler and the distance between patches was decreased by making use of the coupling. A four-beam rectenna with dual-polarizations and dual-spatial coverages was proposed based on the scheme. Another design was a dual-beam rectenna based on a short series-coupled patch array [6]. A periodic circuit model involving coupled resonators is presented and studied for improving the radiation attenuation. The range of RF-to-DC conversion efficiency was 18.5%-44.6% at 2.45 GHz when the input power ranges from -25 to 0 dBm.

Recently, metasurface (MTS)-based antennas have been proposed and analyzed widely because of their properties like low profile, wide operating bandwidth, and high gain [7]-[8]. In a conventional N×N MTS antenna, the unit cells on the MTS layer can be regarded as the radiator. Thanks to these unit cells, single/multiple transverse magnetic (TM) /transverse electric (TE) mode(s) can be excited successfully by using appropriate feeding methods. In particular, it has been proved that, by using appropriate feeding methods, different radiation patterns can be achieved, such as directional, directional with tilted angles, omnidirectional, and end-fire radiation patterns [10]-[13]. It indicates that an MTS antenna has the potential to be excited in different ways to realize the desired radiation pattern.

In addition, the surface-reused or surface-shared technology has been used in the antenna design for minimizing the antenna size or achieving various other functions. In [9], a hybrid RF and solar energy harvesting system utilizing a transparent multi-port patch antenna was presented. The surface area of the solar cell was reused as an antenna to save space. A dual-band MTS-based shared-surface antenna was described in [14]. By exciting unit cells with different feeding methods, a combination of an MTS and a Fabry-Perot surface antenna was proposed.

For MTS antennas, different modes with different radiation patterns can be excited by suitable feeding methods. By exciting these different modes simultaneously, a wide beamwidth antenna can be achieved to harvest more power.

In this paper, a wide-beam rectenna using a multi-port MTS antenna is proposed for energy harvesting at 2.45 GHz. The main contribution is to reuse the unit cells on the MTS layer to excite three modes by three ports simultaneously. This multi-port wide-beam rectenna design increases the effective beamwidth of the antenna without affecting the gain of each beam. A three-branch rectifier circuit is introduced accordingly to rectify and combine received power to a single load. The proposed rectenna achieves a wide beamwidth with a high gain effectively for harvesting more RF energy.

2. Wide-Beam Multi-Port MTS Antenna Design

A. Potential Modes of a Metasurface

Without loss of generality, a typical MTS with 4×4 square elements is shown in Fig. 1. This proposed design is just an example to verify the feasibility of this idea. The MTS antenna with square unit cells is used as a simple example here. It is easier to analyze the modes with square unit cells than other structures because square unit cells are symmetrical along the x- and y-axis.

In this typical MTS antenna design, either TM or TE characteristic modes can be excited on the MTS depending on the feeding structures. For this MTS, the fundamental TM mode (TM_{01}) can be excited for radiation if the feed structure is positioned underneath the middle of the feeding slot between the 2nd and the 3rd column of unit cells. For the TM_{01} mode, the modal current distribution is in phase across the entire MTS [8]; the magnetic field distribution is in phase across the entire MTS, but orthogonal to the modal current distribution. Due to the modal current distribution on the MTS, the radiation pattern will be a directional one. In [7]-[8], a broadside gain of 10 dBi was achieved for an MTS with 4 × 4 elements.

Apart from the fundamental TM_{01} mode, it is also possible to excite higher TM_{xy} modes ($x \geqslant 1$, $y \geqslant 1$) as analyzed in [16]. The choice of the higher TM_{xy} mode is decided by various factors, which will be further discussed in this subsection.

Since the unit cells on the MTS layer are symmetric about the x- and y-axis, there exist pairs of orthogonal higher modes, such as TM_{12} and TM_{21} mode, that can be potentially excited. When the direction of the feeding structure is chosen, only one of the paired modes can be realized.

If the radiation pattern is not a concern, any higher TM_{xy} mode can be considered. However, to complement the directional radiation pattern of the TM_{01} mode, it is desirable to choose those higher TM_{xy} modes with a radiation null in the direction perpendicular to the MTS layer. The reason is that if multiple modes are combined, it will be easier to achieve a wider beamwidth for the combined radiation pattern.

One particular high TM_{xy} mode of interest is described below. For this mode, the modal current distribution is in-phase across the unit cells on the 1st and the 2nd columns. By contrast, the modal current distribution on the 3rd and the 4th column is also in-phase but are out-of-phase with those unit cells on the 1st and the 2nd column. The magnetic field distribution has one closed magnetic field loop along with the vertical gaps in the center. Since the modal current distributions are opposite about the center, this MTS mode has a radiation null in the direction perpendicular to the MTS layer.

Since the modal current distributions of the fundamental TM_{01} mode and this TM_{xy} mode are different, two modes cannot be effectively excited by the same feed simultaneously. In addition, for the higher TM_{xy} mode itself, there are two symmetrical positions where the maximum modal current is maximum, which will induce one main radiation lobe on each side, but a radiation null orthogonal to the MTS layer. This TM_{xy} mode can be excited if one feed structure with two branches is used, with each branch underneath the gap between the 1st and the 2nd column and the gap between the 3rd and the 4th column, respectively.

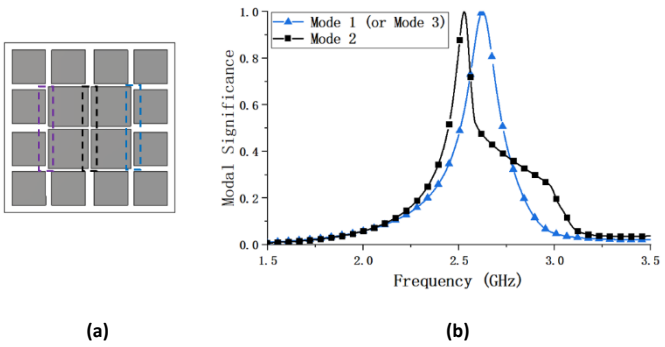

Fig. 1 Configuration of the MTS antenna: (a) the MTS layer and (b) the modal significance of a few modes. A slot on the left-hand side of the ground can excite Mode 1; a slot in the middle can excite Mode 2; a slot on the right can excite Mode 3.

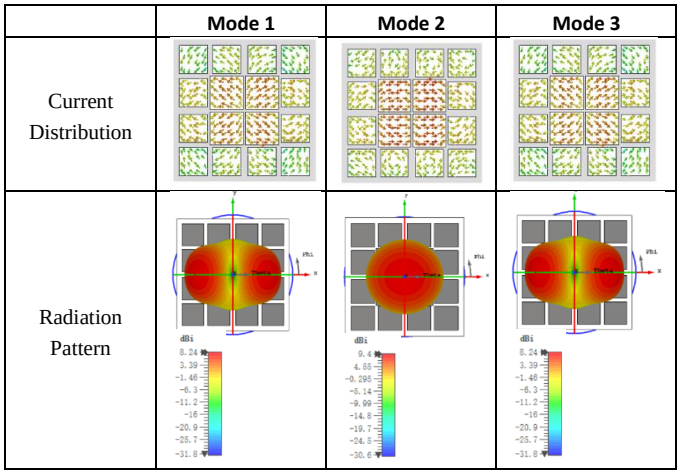

Fig. 2 Modal current distributions and modal radiation patterns of Mode 1, Mode 2, and Mode 3.

A better solution is to decompose this mode with two high-gain radiation lobes into two modes. Each of these two decomposed modes has one main radiation direction. The first decomposed mode is with a stronger current distribution on the 3rd and the 4th column while with a weaker current distribution on the 1st and the 2nd column. Thus, the radiation pattern of this first decomposed mode will have a main lobe inclining along the 1st and the 2nd column and a side lobe inclining along the 3rd and the 4th column. This decomposed mode can be effectively excited by a feed underneath the gap between the 3rd and the 4th column. In contrast, the second decomposed mode has a stronger current distribution on the 1st and the 2nd column while weaker on the 3rd and the 4th column. The radiation pattern of the second decomposed mode will have the main lobe inclining along with the 3rd and the 4th column. The effective feeding position of this decomposed mode is underneath the gap between the 1st and the 2nd column.

To make use of these modes and their associated radiation patterns, three feeding networks with three ports are needed. The dimensions of the MTS elements can be optimized so that the excited decomposed mode will have a similar resonant frequency with the fundamental TM_{01} mode.

These three radiation patterns are generated by three independent feeding ports. Each radiation pattern has a relatively narrow beam but a high gain. For energy harvesting purposes, when a signal is from the left or right, the left or right port can receive the signal with a high gain, respectively. When the signal is from the middle, the centre port can receive the signal with a high gain. The received signal can then be converted to DC individually and combined. Effectively, a rectenna with a high gain and a wide beamwidth is achieved.

B. Mode Analysis of the Proposed Metasurface Antenna

To verify the theory, characteristic mode analysis (CMA) is used to analyze the modes on the proposed MTS layer. Once desired modes are identified, suitable feed structures can be designed to effectively excite these modes.

Normally, in the feed design, it is important to consider the type of the feeding structure and the feeding position. As for the feed type, the aperture-coupled feed type is a conventional method to excite desired modes in an MTS antenna since it can reduce the interference between different layers and is easy to match the impedance [17]-[19]. The apertures on the ground plane can effectively couple electromagnetic energy from the feed to the MTS layer. For the proposed MTS antenna, there are strong modal current distributions at two ends of the unit cells on the MTS layer. If an aperture on the ground plane is positioned right underneath the radiating gap, it can selectively excite the desired mode [12]-[14]. Therefore, three apertures are positioned right underneath the three radiating gaps to excite the three above-mentioned desired modes, respectively.

To reveal the operation mechanism of the proposed MTS antenna, the MTS layer, two substrates, and three apertures on the ground plane are considered. The geometry and layout of the MTS layer remain the same, which are shown in Fig. 1(a). Three feeding positions are shown in Fig. 1(a). The left and right apertures are used to excite Mode 1 (or Mode 3) while the centre aperture is to excite Mode 2.

In CMA, modal significance refers to the importance or contribution of each characteristic mode in a given electromagnetic structure or system. Characteristic modes are the natural resonant modes of an electromagnetic structure and represent the dominant field patterns associated with its eigenfrequencies. The modal significance values are usually obtained by analyzing the modal current distributions associated with each characteristic mode. These current distributions describe the spatial distribution of currents induced within the structure when excited at a particular eigenfrequency. By examining the magnitude of these currents and their distribution, one can determine the relative significance of each mode.

Fig. 1(b) shows the MS's for the proposed MTS with different aperture positions on the ground plane. It is noted that the MS for Mode 1 and Mode 3 are the same since they are symmetrical. It can be seen that the resonant frequencies of Mode 1 (right aperture-coupled feed), Mode 2 (centre aperture-coupled feed), and Mode 3 (left aperture-coupled feed) are all at around 2.45 GHz. Although Mode 1 and Mode 3 are two decomposed high TM_{xy} modes, of which frequencies should be higher than the fundamental mode, the difference between the resonant frequencies of the fundamental mode and the decomposed high TM_{xy} modes is not large. Hence, these three modes can be excited at a similar resonant frequency.

After effectively exciting these three modes, the modal current distributions, and the radiation patterns of Mode 1, Mode 2, and Mode 3 are shown in Fig. 2. It can be seen that the current distribution of Mode 1, the fundamental TM_{01} mode, is in phase across the MTS layer, and the main beam of its radiation pattern is perpendicular to the MTS surface. For Mode 1, the current distribution is in-phase across the unit cells on the 1st and the 2nd columns, but out-of-phase with that on unit cells of the 3rd and the 4th columns. The amplitude of modal current distribution on unit cells of the 3rd and the 4th column is much stronger than that on the 1st and the 2nd column, which is due to the effect of the aperture-coupled feed being on the right. The radiation pattern induced by the modal current distribution is shown in Fig. 2. The main beam is tilted to the left side, and the first side lobe is tilted to the opposite side.

For Mode 3, since it is totally symmetrical with Mode 1, its modal current distribution and radiation pattern are symmetrical with those of Mode 1.

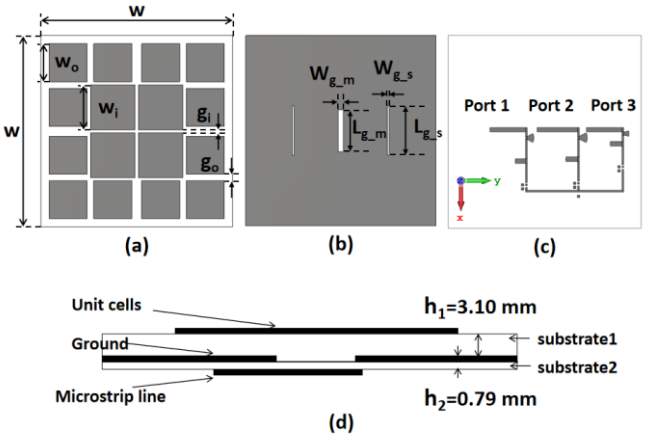

Fig. 3 Geometry of the proposed wide-beam multi-port MTS antenna. (a) Top view of the MTS layer. (b) Top view of the ground plane. (c) Top view of the feed layer. (d) Side view of the whole structure. (w= 120 mm, w_i= 28 mm, w_o= 23.8 mm, g_i= 2 mm, g_o= 6.2 mm, l_{g_m}= 26.6 mm, w_{g_m}= 3.2 mm, l_{g_s}= 31.2 mm, w_{g_s}= 1.2 mm).

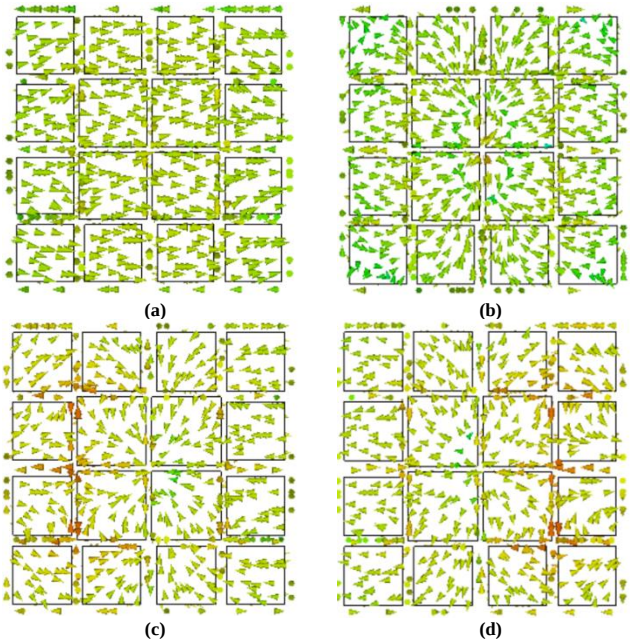

Fig. 4 Current distributions of the proposed MTS antenna on the xoy plane at (a) the fundamental MTS mode (TM_{01}) excited at Port 2, (b) the high mode excited by a feeding structure with two branches, (c) the decomposed higher mode excited at the Port 1, and (d) the decomposed higher mode excited at Port 3.

C. Geometry of the Proposed Metasurface Antenna

To verify the above analysis, a wide-beam and high gain MTS antenna with multiple ports is designed as shown in Fig. 3. The proposed MTS antenna is composed of three layers: the MTS layer, the ground plane layer, and the feeding and rectifying circuit layer. A Rogers RT6002 substrate and a Rogers RT5880 substrate were used to connect these three layers. The heights of the two substrates are 3.1 mm and 0.79 mm, respectively. The geometry and detailed dimensions of the MTS layer and the ground plane layer are shown in Fig. 3.

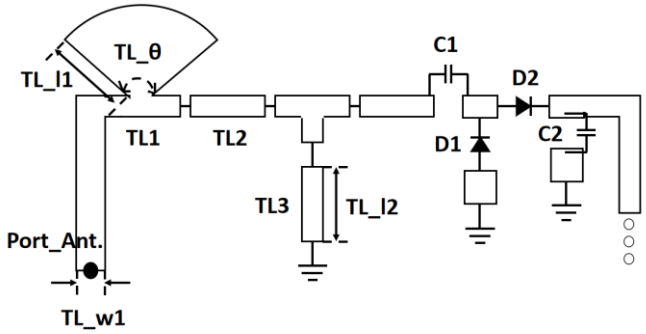

Fig. 5 Topology of a single-branch voltage-doubler rectifying circuit. (TL_w1= 2.5 mm (for all three branches), TL_l1= 3.2/4.8/4.0 mm, TL_l2= 7.3/7.3/6.3 mm, TL_θ= 26.5/52.3/55° (for the left/middle/right branch, respectively), C1= 1000 pF, C2= 100 pF).

On the MTS layer, there are in total 16 unit cells of square metal plates. The sizes of the four inner unit cells are the same and are larger than that of those 12 outer unit cells. For the decomposed modes, if the ratio of the inner cell size and the outer cell size is changed, the resonant frequency, the beamwidth, and the gain will change accordingly. When the ratio is increased, the beamwidth decreases while the gain increases. It is worth noting that this proportional/inverse-proportional relationship does not apply to the fundamental mode. On the ground plane layer, there are three vertical apertures. The positions of these apertures are aligned with the positions of those three vertical gaps between elements on the MTS layer. On the feeding and rectifying circuit layer, three horizontal transmission lines are positioned underneath and orthogonal to the three apertures on the ground plane as feed lines.

Current distributions of the three modes after being excited individually are demonstrated in Fig. 4(a), (c), and (d), respectively. They agree well with the mode analysis by CMA. Fig. 4(b) shows the current distribution of the high TMxy mode when fed by a feeding structure with two branches. In this feeding structure, a power divider is used to split the power into two branches. The positions of the two branches and the coupling apertures for these two branches are very similar to those for Mode 1 and Mode 3. This high TM_{xy} mode is shown here to demonstrate how it can be transformed to Mode 1 and Mode 3.

D. Rectifier Design

Three different modes with different radiation patterns as mentioned above can be incorporated to effectively widen the angle coverage of RF energy harvesting. The harvested RF power needs to be converted to DC and combined to power a single load. The topology and detailed dimensions of a single-branch rectifying circuit are shown in Fig. 5. The circuit consists of a transmission line which is the feed to the antenna, an impedance matching network, and a voltage-doubler rectifying circuit. The DC output was combined with other branches to power a single load.

This rectifier is fabricated on a 0.813-mm-thick RT5880. It is shown as Substrate 2 in Fig. 3(d). The dielectric constant is 2.2 and the loss tangent is 0.0009. In the impedance matching part, the network consists of a radial stub and a short stub, as shown in Fig. 4. The radial stub TL1 is regarded as an open stub, which is equivalent to a variable capacitor by adjusting its angle. This structure can achieve a broadband performance, compared to a quarter-wave stub. The short-circuit stub TL3 is used to cancel the imaginary part of its input impedance, making the real part nearly constant. The matching network is implemented by transmission lines rather than lumped elements to reduce loss. The rectifier consists of two diodes D1 and D2 and two capacitors C1 and C2. Schottky diodes SMS7630 were selected because of their low biasing voltage requirement [15].

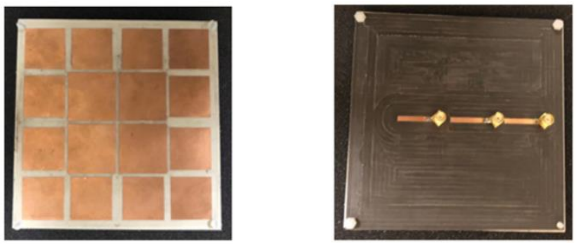

(a) (b)

Fig. 6 Photographs of the fabricated rectenna. (a) Front view. (b) Back view.

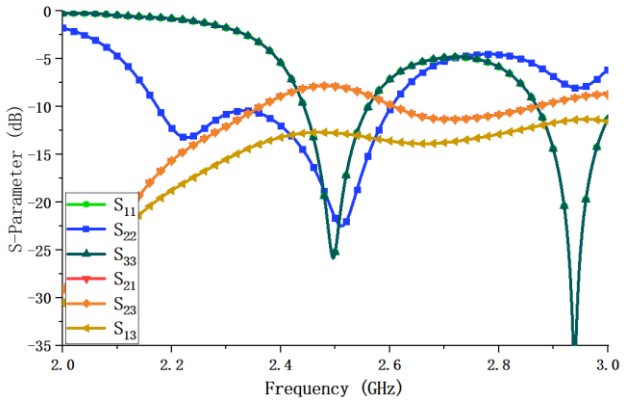

(a)

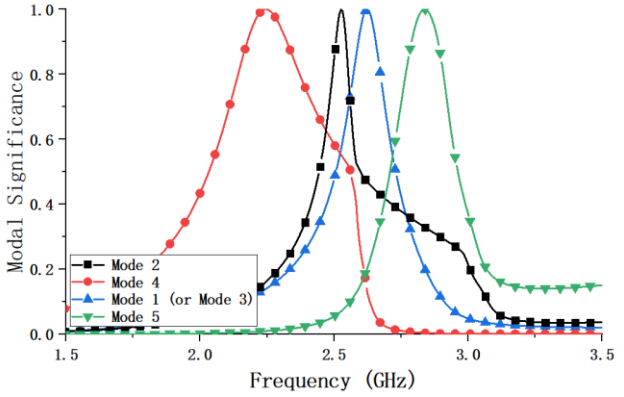

(b)

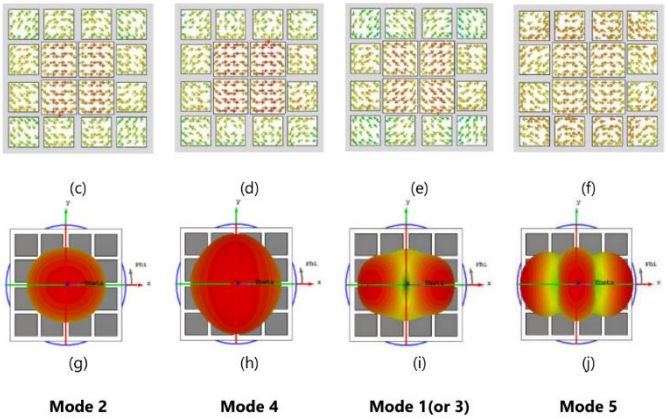

Fig. 7 (a) Simulated reflection coefficients when the antenna is excited by Port 1, Port 2, and Port 3, respectively, and the isolation between Port 1, Port 2, and Port 3 (S_{11}=S_{33} and S_{21}=S_{23}). (b) Modal significance of the proposed MTS antenna. (c)-(j) Modal current distributions and radiation patterns of Mode 1 (or Mode 3), Mode 2, Mode 4 and Mode 5.

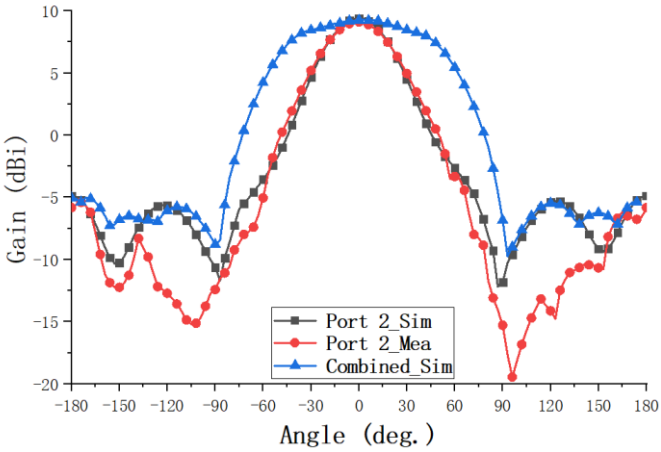

Fig. 8 Simulated and measured gains of the combined structure and in the case when the antenna is excited by Port 2.

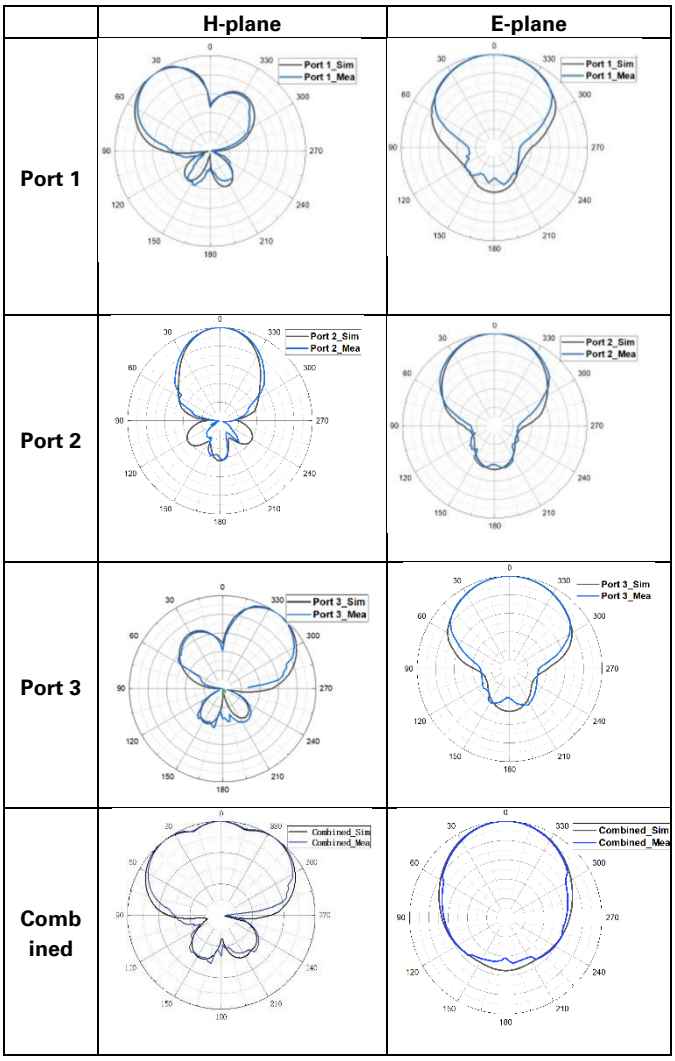

Fig. 9 Simulated and measured normalized radiation patterns at 2.45 GHz when the antenna is excited by Port 1, Port 2, Port 3, respectively, and the effective radiation pattern when they are combined, and the effective radiation pattern when they are combined.

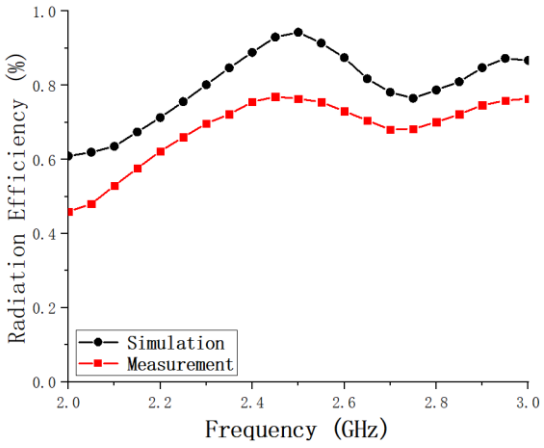

Fig. 10 Simulated and measured radiation efficiency of the antenna when excited by Port 1.

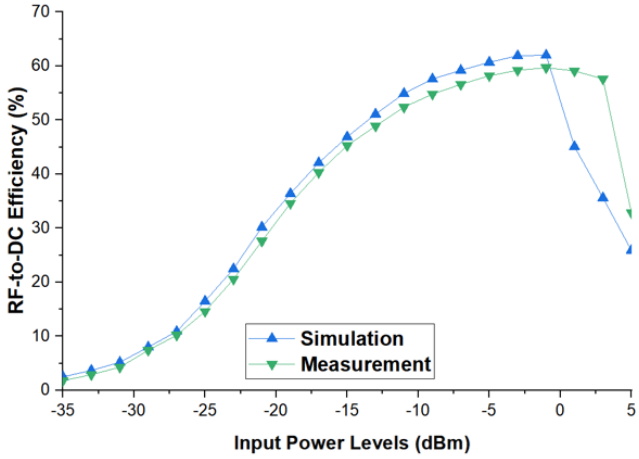

Fig. 11 Simulated and measured RF-to-DC conversion efficiency of the rectifier versus input power at 2.45 GHz with a resistive load.

3. Measurement Result

A. Antenna Measurement

The front and back views of the fabricated MTS antenna are demonstrated in Fig. 6. The simulated and measured S_{11} and gain of the antenna are compared in Fig. 7(a) and Fig. 8, respectively. When the antenna is excited by Port 1, there are two resonances at around 2.5 GHz and 2.9 GHz, respectively. The resonance around 2.5 GHz is Mode 1 (or Mode 3). For Mode 1 (or Mode 3), the current distribution is in-phase across the unit cells on the 1st and the 2nd columns, but out-of-phase with that on unit cells of the 3rd and the 4th columns. The radiation pattern induced by the modal current distribution is shown in Fig. 7(i). There are two beams. One is tilted to the left side, and the other is tilted to the opposite side. When the antenna is excited through Port 3, since it is symmetrical with Port 1, the radiation pattern is very similar to that of the Port 1 case. The resonance around 2.9 GHz is Mode 5, whose radiation pattern has the main lobe in the centre and two side lobes.

When the antenna is excited at Port 2, there are two resonances at 2.2 GHz and 2.5 GHz, respectively. The resonance at around 2.2 GHz is Mode 4. The current distribution of Mode 4 is in phase across the middle of the MTS layer but reversed across the side patches. So, the radiation pattern is directional in the centre and has two side lobes. The resonance at 2.5 GHz is Mode 2. The current distribution of Mode 2 is in phase across the whole MTS layer. Thus, the radiation pattern of Mode 2 is very directional.

Based on the above analysis, Mode 1(or 3) and Mode 4 are desired and chosen for energy harvesting applications. Then, appropriate feeding structures are selected to successfully excite these modes. It is clear from Fig. 7(d) that the maximum current distribution of Mode 4 is at the vertical centre of the MTS layer, so an aperture could be cut on the ground plane to excite the desired Mode 4. Due to the small size of this vertical aperture, the CMs are not affected significantly.

The simulated bandwidth of the MTS antenna with a better than -10 dB reflection coefficient is 19.6% when the antenna is excited at Port 2, and 7% when excited by Port 1 and Port 3. While the measured one is 22% at Port 2, and 12% at Port 1 and Port 3. The measured bandwidth is much wider than the simulated one because of the loss of the substrate and conductor.

The isolation between Port 1 (or Port 3) and Port 2 is 8 dB in both the simulation and the measurement. The isolation between Port 1 and Port 3 is 12.7 dB. For energy harvesting applications, it is not necessary for each port of the proposed antenna to be perfectly isolated from others. This is because a rectifier is added after each port. Even if the energy is coupled from one port to the other due to low isolation, the energy will be combined in the output of the proposed design eventually anyway. The isolation level achieved can also ensure that the radiation patterns will not be significantly affected and the antenna performance will not be greatly degraded due to the cross coupling.

The simulated and measured gains when the antenna is excited by the centre and the two side ports are 9.5 dBi and 8.7 dBi, respectively. As shown in Fig. 8 and Fig. 9, the maximum gain of the antenna when excited by the centre side port is similar to the maximum gain of the combined pattern. But the beamwidth of the combined pattern is much larger than that of the case when excited at the center or side port. Due to the dielectric loss and fabrication tolerance, the measured radiation efficiency of the MTS antenna is slightly lower than the simulated one. The simulated radiation efficiency of the antenna when excited by Port 1 is from 0.61 to 0.93 while the measured radiation efficiency is from 0.47 to 0.76, as shown in Fig. 10. The reason why the simulated and measured radiation efficiencies in Fig. 10 are different is as follows. The material used in the CST simulation is lossless while the material used in the measurement has both metallic (copper) loss and substrate (dielectric) loss.

Fig. 9 shows the simulated and measured normalized radiation patterns of the MTS antenna at 2.45 GHz. The tilted angles of the H-field radiation patterns when excited by each port are at +35°, 0°, and -35°, respectively. The combined pattern in Fig. 9 is the result of numerical calculation. The total output power is the sum of the output power from the three ports. The beamwidth for each port is around 46°. For energy harvesting applications, when the DC output powers from the three ports are combined, a wide beamwidth of 117° can be achieved, effectively. The beamwidths of the three modes in the E-planes are similar, at around 90°. The measured normalized radiation patterns are all in good agreement with the simulated results. In addition, it is noted that the back lobe levels in Fig. 9 are slightly lower than that in Fig. 2. This is because the radiation pattern in Fig. 2 is the result of CMA. Only the metasurface layer and the ground layer were considered in the analysis. The excitation circuit was not considered in the analysis. By contrast, the radiation pattern in Fig. 9 is the result of full-wave simulation of the whole antenna structure including the metasurface layer, the ground layer and the feeding transmission line. The two results are from two different structures; therefore, the back lobe levels are slightly different.

B. Rectifier Measurement

Three rectifiers are connected to Port 1, Port 2, and Port 3 of the MTS antenna, respectively, for RF-DC conversion. The output DC voltage V_{DC} of the rectifier is measured across the resistive load R_L. To evaluate the RF-to-DC conversion efficiency of the rectifier, the rectifier is connected to a signal generator Keithley 2920, and a multimeter is used to measure V_{DC}. The RF input

power was from -35 to 5 dBm at 2.45 GHz. The RF-to-DC conversion efficiency of the rectifier can be obtained from

$$\eta = \frac{{V_{DC}}^2}{R_L} \times \frac{1}{P_{in}} \quad (1)$$

where Pin denotes the input RF power provided by the signal generator. The measured RF-to-DC conversion efficiency of the rectifier versus input RF

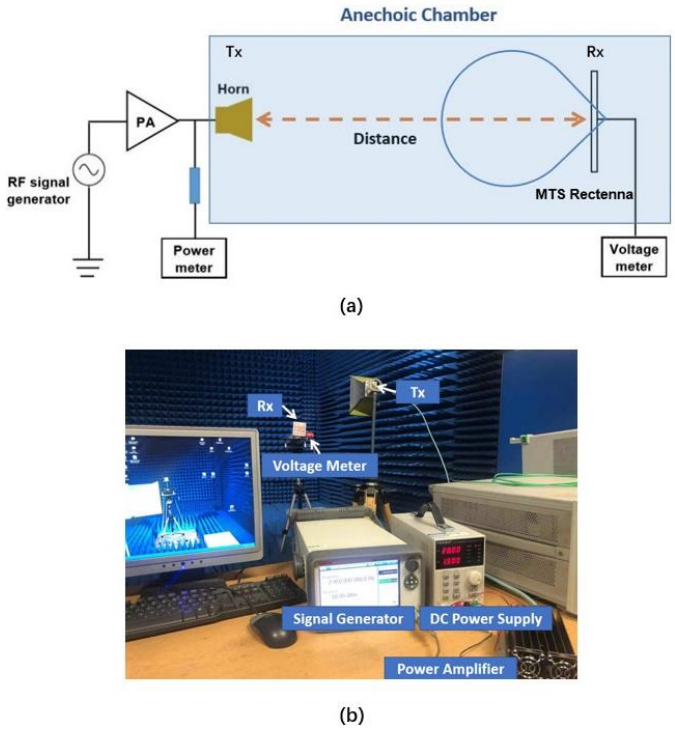

Fig. 12 (a) Diagram and (b) photograph of the measurement setup.

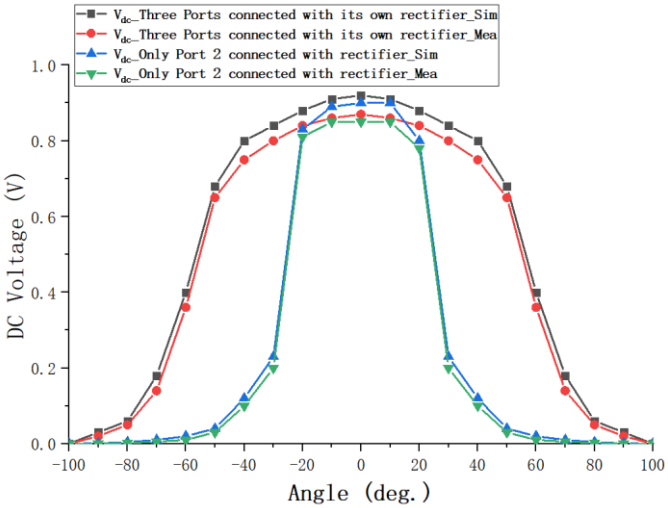

Fig. 13 Simulated and measured DC output voltage at different incident angles.

power levels are plotted in Fig. 11. It can be seen that, for the rectifying circuit with a single load resistance, the maximum conversion efficiency is 63% at -1 dBm, and over 30% when the input power level is higher than -20 dBm. This rectifier circuit can still work with an efficiency of around 1.5% at a low input RF power level of -35 dBm. In this rectifier design, a nonlinear model is used to represent the diodes, so the parasitic effect and extra loss were considered in the simulation.

C. Rectenna Measurement

The measurement setup of the rectenna is shown in Fig. 12. The source signal was generated by a Keithley 2920 RF signal generator and was amplified by a 43 dB gain power amplifier. The signal was transmitted by a calibrated horn antenna. The proposed rectenna was used to receive the signal at a distance of 1 m from the transmit antenna. The front and back views of the proposed rectenna are shown in Fig. 6. The power delivered to the transmit antenna was measured by a power meter while the received power by the rectenna was calculated using the Friis transmission equation [20]:

$$P_r = P_t + G_t + G_r + 20\,log_{10}\frac{\lambda}{4\pi r} \quad (2)$$

where P_r is the received power in dBm, P_t is the transmit power in dBm (43), G_t is the gain of the horn in dBi (9.8), G_r is the gain of the proposed rectenna in dBi, λ is the free space wavelength at 2.45 GHz, and r is the distance between the transmitter and the receiver in meter (1).

The measurement was carried out in an anechoic chamber. The rectenna was rotated over a 180° range in order to vary the incident angle of the RF radiation on the rectenna. The DC output voltage was measured after every 5° rotation. The total RF-to-DC conversion efficiency of the rectenna could then be calculated. The combined output DC voltage was simulated and measured respectively, as shown in Fig. 13. The measured output DC voltage was over 0.7 V within an angle range of -50° to +50° and was over 0.3 V from -60° to +60°. The measured beamwidth of the receiver is around 100° because of the fabrication inaccuracy. It is noted that the simulated 3 dB beamwidth of the rectenna is around 117°, which is the combination of the beamwidths of Port 1, Port 2, and Port 3. The effective beamwidth of the proposed rectenna is 2.5 times that of the rectenna with a single port. This consequently verified that an extended angle coverage range could be achieved with the proposed design method.

In Table I, the achieved results are compared with other multi-port rectennas designed for energy harvesting from low-power RF sources. The gain of the proposed MTS rectenna, when excited by individual ports, is comparable with that of other rectennas. Compared with [14], the proposed rectenna has a much simpler structure, smaller dimensions, and a wider beamwidth. By using a grid-array antenna in [5], the size of the whole rectenna is five times bigger than the proposed rectenna. Compared with the rectenna design with a similar size, the beamwidth of our rectenna is 30% wider than that in [6]. In addition, a high gain rectenna is proposed in [21] but the rectenna size is very big compared with our proposed antenna. The rectenna design in [22] has a bigger size and a lower gain, although the RF-to-DC conversion efficiency is higher.

4. Conclusions

Table 1 – Comparison of the Proposed Rectenna with Related Designs.

Ref.	Rectenna Dimension (in terms of λ_0)	Complexity of the Overall Design	Frequency (GHz)	Overall -3dB beamwidth (°)	Peak Gain (dBi)	RF-to-DC conversion efficiency (%)
[14]	$2.0\lambda_0 \times 0.83\ \lambda_0 \times 0.04\ \lambda_0$	Complex	2.45	Center lobe: 80 Side lobe: 80	8.7	42.4% (input power= -10 dBm) 55.3% (input power= -4 dBm)
[5]	$1.2\lambda_0 \times 0.78\lambda_0 \times 0.03\ \lambda_0$	Simple	2.45	Each beam (2): 90	10.10	13.8% – 51.0% (Power density=1 μW/cm^2)
[6]	$1.25\lambda_0 \times 0.67\lambda_0 \times 0.03\ \lambda_0$	Simple	2.45	Each beam (2): 90	8.53	19.5% – 44.6% (Power density: 0.05-1 μW/cm^2)
[21]	$1.5\lambda_0 \times 1.5\lambda_0 \times 0.27\ \lambda_0$	Complex	7.5	Each beam (4): 30±2	10.8	N/A
[22]	$2.5\lambda_0 \times 2.5\lambda_0 \times 0.03\ \lambda_0$	Complex	5.8	Each beam (6): 57	5.2	65.28%/69.1%
This Work	$\lambda_0 \times \lambda_0 \times 0.03\ \lambda_0$	Simple	2.45	117	7.8	47.4% (Power density=1 μW/cm^2, input power: -35-0 dBm)

It has been presented that it is possible to achieve high gain and effectively a wider beamwidth simultaneously by reusing MTS-based antennas for energy harvesting. Different MTS modes having high gain radiation patterns can be excited individually with their outputs combined. For example, when the electromagnetic waves are from the left side, the MTS mode with a main lobe on the left can receive the electromagnetic energy with a high gain. If the electromagnetic waves are vertical to the MTS layer, the fundamental mode with a directional main lobe orthogonal to the MTS layer can harvest energy with a high gain. Therefore, it can effectively receive electromagnetic waves from a wide angle. At the same time, the receiver part is low-profile and with simple structures permitting easy implementation. This rectenna design is particularly suitable for scenarios where the source location is unknown or multiple sources co-exist from different directions.

References

[1] S. -J. Kim, S. Kim, J. -H. Lee and J. -W. Yu, "A Compact RF Energy Harvesting System With an Improved Impedance Matching Network," in *IEEE Antennas and Wireless Propagation Letters*, doi: 10.1109/LAWP.2023.3323355.

[2] D. Surender et al., "Analysis of Facet-Loaded Rectangular DR-Rectenna Designs for Multisource RF Energy-Harvesting Applications," in *IEEE Transactions on Antennas and Propagation*, vol. 71, no. 2, pp. 1273-1284, Feb. 2023, doi: 10.1109/TAP.2022.3231014.

[3] A. M. Jie, Nasimuddin, M. F. Karim and K. T. Chandrasekaran, "A Wide-Angle Circularly Polarized Tapered-Slit-Patch Antenna With a Compact Rectifier for Energy-Harvesting Systems [Antenna Applications Corner]," in *IEEE Antennas and Propagation Magazine*, vol. 61, no. 2, pp. 94-111, April 2019, doi: 10.1109/MAP.2019.2895648.

[4] S. Shen, Y. Zhang, C. -Y. Chiu and R. Murch, "A Triple-Band High-Gain Multibeam Ambient RF Energy Harvesting System Utilizing Hybrid Combining," in *IEEE Transactions on Industrial Electronics*, vol. 67, no. 11, pp. 9215-9226, Nov. 2020, doi: 10.1109/TIE.2019.2952819.

[5] Y. -Y. Hu, S. Sun, H. Wu, S. Yang and J. Hu, "Integrated Coupler-Antenna Design for Multibeam Dual-Polarized Patch-Array Rectenna," in *IEEE Transactions on Antennas and Propagation*, vol. 70, no. 3, pp. 1869-1883, March 2022, doi: 10.1109/TAP.2021.3111197.

[6] Y. -Y. Hu, S. Sun, H. -J. Su, S. Yang and J. Hu, "Dual-Beam Rectenna Based on a Short Series-Coupled Patch Array," in *IEEE Transactions on Antennas and Propagation*, vol. 69, no. 9, pp. 5617-5630, Sept. 2021, doi: 10.1109/TAP.2021.3069425.

[7] D. Manteuffel, F. H. Lin, T. Li, N. Peitzmeier and Z. N. Chen, "Characteristic Mode-Inspired Advanced Multiple Antennas: Intuitive insight into element-, interelement-, and array levels of compact large arrays and metantennas," in *IEEE Antennas and Propagation Magazine*, vol. 64, no. 2, pp. 49-57, April 2022, doi: 10.1109/MAP.2022.3145714.

[8] J. F. Gao and F. H. Lin, "Modeling and Analysis of Wideband Multilayer Metasurface Antenna Array Using Characteristic-Mode Analysis," in *IEEE Transactions on Antennas and Propagation*, vol. 71, no. 3, pp. 2832-2836, March 2023, doi: 10.1109/TAP.2023.3234201.

[9] Y. Zhang, S. Shen, C. Y. Chiu and R. Murch, "Hybrid RF-Solar Energy Harvesting Systems Utilizing Transparent Multiport Micromeshed Antennas," in *IEEE Transactions on Microwave Theory and Techniques*, vol. 67, no. 11, pp. 4534-4546, Nov. 2019, doi: 10.1109/TMTT.2019.2930507.

[10] L. Liu et al., "A Broadband Circularly Polarized Antenna Based on Transparent Conformal Metasurface," in *IEEE Antennas and Wireless Propagation Letters*, doi: 10.1109/LAWP.2023.3316427.

[11] W. Yang, S. Chen, W. Che, Q. Xue and Q. Meng, "Compact High-Gain Metasurface Antenna Arrays Based on Higher-Mode SIW Cavities," in *IEEE Transactions on Antennas and Propagation*, vol. 66, no. 9, pp. 4918-4923, Sept. 2018, doi: 10.1109/TAP.2018.2851659.

[12] Z. N. Chen et al., "Microwave Metalens Antennas," in *Proceedings of the IEEE*, vol. 111, no. 8, pp. 978-1010, Aug. 2023, doi: 10.1109/JPROC.2023.3287599.

[13] T. Li and Z. N. Chen, "Wideband Substrate-Integrated Waveguide-Fed Endfire Metasurface Antenna Array," in *IEEE Transactions on Antennas and Propagation*, vol. 66, no. 12, pp. 7032-7040, Dec. 2018, doi: 10.1109/TAP.2018.2871716.

[14] T. Li and Z. N. Chen, "Shared-Surface Dual-Band Antenna for 5G Applications," in *IEEE Transactions on Antennas and Propagation*, vol. 68, no. 2, pp. 1128-1133, Feb. 2020, doi: 10.1109/TAP.2019.2938584.

[15] C. Song, Y. Huang, P. Carter, J. Zhou, S. D. Joseph and G. Li, "Novel Compact and Broadband Frequency-Selectable Rectennas for a Wide Input-Power and Load Impedance Range," in *IEEE Transactions on Antennas and Propagation*, vol. 66, no. 7, pp. 3306-3316, July 2018, doi: 10.1109/TAP.2018.2826568.

[16] T. Li and Z. N. Chen, "Wideband Sidelobe-Level Reduced Ka -Band Metasurface Antenna Array Fed by Substrate-Integrated Gap Waveguide Using Characteristic Mode Analysis," in *IEEE Transactions on Antennas and Propagation*, vol. 68, no. 3, pp. 1356-1365, March 2020, doi: 10.1109/TAP.2019.2943330.

[17] W. Zhao, X. Li, Z. N. Chen and Z. Qi, "Broadband and High-Gain Embedded Probe-Fed Low-Profile High-Order-Mode Antennas," in *IEEE Transactions on Antennas and Propagation*, vol. 71, no. 9, pp. 7609-7614, Sept. 2023, doi: 10.1109/TAP.2023.3291813.

[18] Y. -H. Lv, Z. N. Chen, R. Wang and B. -Z. Wang, "Dual-Polarized Multiresonant Metantenna for Quasi-Independent Radiation and In-Band Scattering Manipulation," in *IEEE Transactions on Antennas and Propagation*, vol. 71, no. 7, pp. 5895-5908, July 2023, doi: 10.1109/TAP.2023.3281059.

[19] F. H. Lin and Z. N. Chen, "Resonant Metasurface Antennas With Resonant Apertures: Characteristic Mode Analysis and Dual-Polarized Broadband Low-Profile Design," in *IEEE Transactions on Antennas and Propagation*, vol. 69, no. 6, pp. 3512-3516, June 2021, doi: 10.1109/TAP.2020.3028246.

[20] I. A. Shah, M. Zada, S. A. A. Shah, A. Basir and H. Yoo, "Flexible Metasurface-Coupled Efficient Wireless Power Transfer System for Implantable Devices," in

IEEE Transactions on Microwave Theory and Techniques, doi: 10.1109/TMTT.2023.3319050.

[21] J. Luo, L. Li, J. Su, R. Ma, G. Han and W. Zhang, "Multibeam Antenna Based on Partially Reflecting Defected Metasurface," in *IEEE Antennas and Wireless Propagation Letters*, vol. 20, no. 8, pp. 1582-1586, Aug. 2021, doi: 10.1109/LAWP.2021.3091608.

[22] M. Kumar, S. Kumar, A. S. Bhadauria and A. Sharma, "A Planar Integrated Rectenna Array With 3-D-Spherical DC Coverage for Orientation-Tolerant Wireless-Power-Transfer-Enabled IoT Sensor Nodes," in *IEEE Transactions on Antennas and Propagation*, vol. 71, no. 2, pp. 1285-1294, Feb. 2023, doi: 10.1109/TAP.2022.3228708.

.